Zhou *et al.*
Chinese Journal of Mechanical Engineering (2023) 36:27
https://doi.org/10.1186/s10033-023-00853-1

Chinese Journal of Mechanical Engineering

ORIGINAL ARTICLE

Open Access

Micro-Sized Pinhole Inspection with Segmented Time Reversal and High-Order Modes Cluster Lamb Waves Based on EMATs

Jinjie Zhou[1*], Yang Hu[1], Xiang Li[2], Yang Zheng[3], Sanhu Yang[1] and Yao Liu[1]

Abstract

Pinhole corrosion is difficult to discover through conventional ultrasonic guided waves inspection, particularly for micro-sized pinholes less than 1 mm in diameter. This study proposes a new micro-sized pinhole inspection method based on segmented time reversal (STR) and high-order modes cluster (HOMC) Lamb waves. First, the principle of defect echo enhancement using STR is introduced. Conventional and STR inspection experiments were conducted on aluminum plates with a thickness of 3 mm and defects with different diameters and depths. The parameters of the segment window are discussed in detail. The results indicate that the proposed method had an amplitude four times larger than of conventional ultrasonic guided waves inspection method for pinhole defect detection and could detect micro-sized pinhole defects as small as 0.5 mm in diameter and 0.5 mm in depth. Moreover, the segment window location and width (5—10 times width of the conventional excitation signal) did not affect the detection sensitivity. The combination of low-power and STR is more conducive to detection in different environments, indicating the robustness of the proposed method. Compared with conventional ultrasonic guided wave inspection methods, the proposed method can detect much smaller defect echoes usually obscured by noise that are difficult to detect with a lower excitation power and thus this study would be a good reference for pinhole defect detection.

Keywords Pinhole corrosion, High-order modes cluster, Lamb waves, Segmented time reversal inspection, Electromagnetic acoustic transducer

1 Introduction

The unreachable areas of plates and pipes are often more likely to produce pinhole-type pitting corrosion, such as the bottom regions of pressure vessels and support locations where liquids, air, and local stress are coupled. With increasing service time, pitting corrosion leads to through-thickness pinhole damage and increases leakage risk. Pinhole corrosion smaller than 1 mm are difficult to detect, even on the visible surfaces of plates and pipes. As for the defects in inaccessible regions, it is more difficult to evaluate. These kinds of structures are usually used to store and transport hazardous chemicals and gasses, the leakage or rupture may lead to tremendous accidents. Therefore, it is critical to accurately detect and evaluate pinhole corrosion to ensure the safe operation of equipment.

Fortunately, the ultrasonic guided waves have long range propagation ability and can detect defects at inaccessible regions that cannot be detected by ultrasonic body waves [1, 2]. However, low frequency guided waves are often used for long-range rough inspection and are unsuitable for pinhole defect detection because of its low resolution due to long wavelength [3–5]. The high-order

*Correspondence:
Jinjie Zhou
zhoujinjiechina@126.com
[1] School of Mechanical Engineering, North University of China, Taiyuan 030051, China
[2] School of Aeronautics and Astronautics, University of Electronic Science and Technology of China, Chengdu 611731, China
[3] China Special Equipment Inspection and Research Institute, Beijing 100029, China

modes cluster (HOMC) consists of higher order Lamb wave modes that travel together with similar group velocities to form a cluster and remain practically non-dispersive at long distances [6].

Furthermore, compared with that of the piezoelectric method [7–9], the electromagnetic acoustic transducers (EMATs) are non-contact, free of couplants and require no surface polishing, especially easier to excite different guided waves modes. Flexible modes excitation of EMATs is more applicable to special areas such as plates and pipes support regions. Hence, a HOMC based on EMATs at high frequencies has high resolution, which is a potential effective method for detecting small pinhole corrosion.

The key issues of HOMC are high frequency modes selection and operating point determination of guided waves. For high-frequency guided waves, Ratnam et al. [10] detected hole defects with a diameter of 10 mm and a depth of 2 mm in aluminum plates using 1.3−2.2 MHz EMATs. Nurmalia et al. [11] conducted higher order mode detection on 3 mm thick aluminum tubes with diameters of 25 mm and found a defect with a 0.5 mm depth and 12.6 mm diameter. Through simulations and experiments, Liu et al. [12] found that defects could be detected selectively by changing the magnet polarization angle to excite A1 mode-guided waves in a plate at 2.25 MHz. Related work has mainly focused on the analysis of the constituent modes in the HOMC. Reddy et al. [13] used DISPERSE to obtain the displacement profile of individual modes across a plate thickness and used a genetic algorithm to optimize the weights of each mode. High order modes, such as center frequencies at 1.0 MHz and 2.25 MHz and frequency × thickness products of 18 MHz·mm and greater than 20 MHz·mm, respectively, were used for these small defects. Defects as small as 1.5 mm in diameter, 0.5 mm in depth and 0.8 mm^2 in area were detected. However, no detections of 0.5 mm × 0.5 mm (diameter × depth) pinhole corrosion defects have been reported. In this situation, the SNR and accuracy will be low. From another perspective, EMAT inherent low effectiveness also causes lower SNR and makes micro-sized pinhole detection difficult. This calls for a reliable detection technique capable of using signal processing methods.

The time-reversal (TR) method has a spatio-temporal focusing effect and can be used to enhance the micro-sized defect inspection. Gangadharan et al. [14] proved the effectiveness of Lamb waves in TR detection by detecting a 10 mm × 2 mm defect. Zhang et al. [15] used the 700 kHz L(0, 2) mode for the TR detection of 1-mm deep defects and obtained a clear echo, improving the detection ability of pitted corrosion. Harley et al. [16] used the TR method to detect artificial defects with dimensions of 1 mm × 1 mm × 25 mm (depth × width × length). Guan et al. [17] tested a 2-mm diameter defect in a 1-mm thick aluminum plate using the TR method and obtained a higher precision than traditional methods. Xu et al. [18] used the focusing effect of the TR inspection to detect and locate a 2 mm × 3 mm (width × depth) notch defect. Zhang et al. [19] used the focusing principle of TR on Lamb waves to detect damage 15 mm in diameter. Although these methods can detect small defects to varying degrees, no method can effectively detect micro-sized pinhole defects less than 1 mm in size, which often occurs in inaccessible structures. Furthermore, the methods used in the above conventional TR studies did not combine their methods with the HOMC technique and take advantage of high-frequency technology.

In contrast to conventional TR methods, some improvements have been made to enhance the SNR of defect detection techniques [20–23]. Much research has investigated TR operators using comprehensive theoretical and experimental methods, such as extracting narrowband responses by wavelets [24] and controlling the frequency bandwidth of narrow excitation signals [25]. Moreover, the relationship between the parameters and reconstructed quality was investigated through excitation frequency, bandwidth and piezoelectric geometry [26]. Some studies have analyzed the effects of adhesives, tone burst count and piezoelectric thickness [27]. However, they did not provide a compensation method. Huang et al. [28] proposed a frequency-dependent compensation method by placing a weight vector on its spectrum. In addition to alleviating the frequency-dispersion impact, some researchers have focused on the use of multiple frequencies [29] and combining the TR operator with a multiple-signal classification method to yield a pseudo-spectrum [30]. These methods can achieve super-resolution imaging and can be applied to medical imaging. Therefore, the TR focusing method is an efficient method for locating and sizing defects.

In pinhole corrosion applications, the information of micro-sized defects contained in a structure is often submerged in noise and is difficult to identify. The TR method does not need to scan point-by-point, but it needs to judge the approximate location of defects in advance. Deng et al. [31, 32] performed TR detection for different types of cracks by studying the interception of a 60−180 μs TR-window width. They found that the amplitude of the defect echo first increased and then decreased with an increase in TR window width. Therefore, a wide TR window is not conducive to detection. When the TR-window is set to a small width, the approximate position of the defect must be determined in advance, and an appropriate starting point of the TR-window must

be set to ensure that the window contains an echo from the defect. Combining the above two focusing methods, a new method of segmented time reversal (STR) detection is proposed in this study. First, the detection interval is divided into some segments, and then the TR signal of each interval is re-excited to obtain the TR detection signal of each segment. The STR method aims to solve the problem that normal TR methods are difficult to determine the starting point of a narrow TR window.

In this study, a new micro-sized pinhole detection method with HOMC Lamb waves and STR based on EMATs is proposed to detect the defects of less than 1 mm. The advantage of the proposed method is first presented in theory, and HOMC Lamb waves at 2.87 and 3.96 MHz were selected. A detection test on aluminum plates with several artificial pinhole defects is conducted to prove the superiority and high sensitivity of proposed method compared with that of the conventional inspection method used to detect micro-sized defects (0.5 mm × 0.5 mm). Subsequently, the effects of the segmented window location and width on the inspection results are analyzed to reveal the robustness of this highly sensitive (high SNR) method. Finally, the parameters of the excitation power are tested by using the proposed method to deal with the EMATs scenario with a lower SNR.

2 Theory

2.1 Basic Theory of STR Method

According to theoretical studies of conventional TR Lamb waves in plate-like structures [33], the STR method for the HOMC is illustrated in Figure 1. Two EMATs were attached to the surface of the plate in a pitch-catch configuration. The transmitting transducer (Transducer T) was excited by the signal from the experimental system to generate guided waves that were transmitted to the receiving transducer (Transducer R) through the inspected specimen. Then, the response signal at Transducer R was divided into several segments in the time domain and reversed for application to Transducer R. The roles of the transmitting and receiving transducers were interchanged. The STR signals were used as the excitation signal and transmitted from the Transducer R to Transducer T. The TR response signal collected from Transducer T was used to reconstruct the signal and identify the defect.

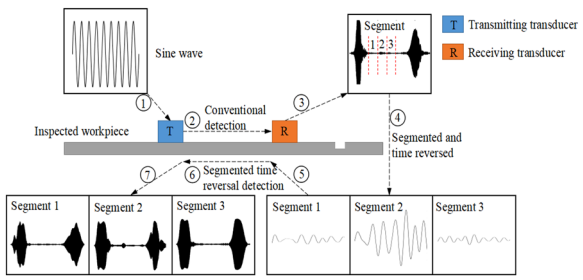

Figure 1 Diagram of STR method

As shown in Figure 1, when an excitation signal $V_T(w)$ was applied to Transducer T, the response signal $V_R(w)$ at Transducer R in the frequency domain after guided waves propagation in the inspected specimen can be expressed as:

$$V_R(w) = V_T(w)K_TK_RH(d,w), \tag{1}$$

where w is the angular frequency; K_T and K_R are the energy conversion efficiencies of the transmitting and receiving transducers, respectively, and d and $H(d, w)$ are the distance and guided waves transfer functions between Transducers T and R, respectively.

When $V_T(w)$ has a certain frequency bandwidth and each frequency component on the dispersion curve produces a phase difference, the response signal inevitably exhibits frequency dispersion. Reversal of the response signal in the time domain is equivalent to the complex conjugation in the frequency domain. The TR response signal is:

$$V_R^*(w) = V_T^*(w)K_T^*K_R^*H^*(d,w), \tag{2}$$

where X^* represents the conjugation complex of X. When the TR signal is applied to Transducer R, it is treated as a new transmitting transducer. According to the reciprocity principle of acoustic wave propagation, as the structure and position of Transducers R and T remain unchanged, the frequency response of the transfer function remains. Then, the response signal received by Transducer T after the TR inspection process is:

$$\begin{aligned} V_T^1(w) &= V_R^*(w)K_TK_RH(d,w) \\ &= V_T^*(w)K_T^*K_R^*K_TK_RH^*(d,w)H(d,w) \\ &= V_T^*(w)K_{TR}H_{TR}(d,w), \end{aligned} \tag{3}$$

where $K_{TR} = K_T^*K_R^*K_TK_R$; and $H_{TR}(d,w) = H^*(d,w)H(d,w)$.

According to Eq. (3), the response signal received by Transducer T does not contain a phase delay factor, which means that TR process can compress the guided waves frequency dispersion and focus the frequency on the operation points. $K_{TR}H_{TR}$ is the multiplication of conjugate complex numbers and is a real, even, positive function. The inverse Fourier transform at the zero point in time is an in-phase superposition.

For the segmented signal, $H(d, w)$ can be written as:

$$H(d,w) = \beta A(d,w)e^{-ik(w)d}, \tag{4}$$

where β is reflection coefficient for the defect echo, $A(d, w)$ is the amplitude function of the guided waves mode, $k(w)$ is the wave number of the guided waves mode, and

e^{-ikwd} is the phase delay factor of the guided waves mode. Then, the transfer function in the TR inspection H_{TR} can be presented as:

$$H_{TR}(d,w) = \beta^2 \left|A(d,w)\right|^2. \tag{5}$$

If the TR window contains defect echoes, its coefficient changes to β^2, and the energy of the TR signal at the defects is enhanced because of $\left|A(d,w)\right|^2$. If the TR window does not contain defect echoes, there is only noise in the excitation waveform. Therefore, the SNR of TR inspection signal is very low, and no effective signal can be distinguished.

2.2 Principle of HOMC Lamb Waves Excited by EMATs

Because the group velocities between neighboring HOMC Lamb waves are almost the same, various modes generated at the specific frequency will form a unique wave packet. The HOMC Lamb waves mode with a short wavelength has sub-millimeter resolution and sensitivity suitable for identifying micro-sized pinhole defects. When Lamb waves were excited at improper frequency, multiple modes could be generated simultaneously, which leads to the overlap of inspection signals and make the mode separation very difficult. Therefore, the selection of appropriate Lamb wave modes and specific operating points of guided waves on dispersion curves should be considered, and the principle of HOMC excitation by EMATs should be considered systematically.

The Lamb wave modes used in this study were generated by the EMATs with meander-line coils. The design of meander-line coils in an EMAT should satisfy the relationship among the phase velocity, excitation frequency, and line spacing of the coils, which are:

$$d = \frac{\lambda}{2}, \lambda = \frac{Cp}{f}, \lambda = P, \tag{6}$$

where d is the line spacing of the coils, λ is the wavelength, Cp is the phase velocity, f is the frequency of operating point, and P is the spatial period of the coil which is the same as λ.

3 Experiment Setup

3.1 Excitation Frequency Selection

To determine the inspection frequency of the Lamb wave mode in an aluminum plate with a thickness of 3 mm, the relationship between frequency and phase velocity was first calculated as shown in Figure 2. A black line with a slope of wavelength λ was added in Figure 2 to generate a lot of intersection points with the Lamb waves mode. The intersection points are the potential excitation points of the Lamb waves due to inner structure and characterization of the designed EMATs. However, many modes exist in the high-frequency region. Even if the frequency at the intersection points is used as the excitation frequency, other modes will also be excited. When selecting the excitation frequency, the degree of frequency dispersion should be considered. The point with low frequency dispersion, which is the segment with a low slope in the phase velocity curve, should be preferentially selected owing to the high focus rate on the mode.

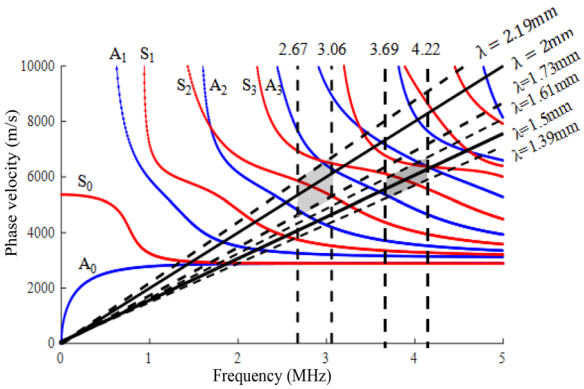

Figure 2 Dispersion curve and excitation region of Lamb waves phase velocity for 3 mm aluminum plate

Assuming a coil spacing of 1 mm, the wavelength of Lamb waves is 2 mm. Based on the dispersion curve in Figure 2, a wave of 2.87 MHz was selected as the excitation signal. When the main energy of the excitation signal spectrum declines to half, the decided frequency bandwidth range and wavelength bandwidth are 2.67−3.06 MHz and 1.73−2.19 mm respectively. The intersection area of the frequency and wavelength bandwidth marked in gray in Figure 2 is the excitation area of Lamb waves, which mainly includes the S_2 mode. The excitation frequency is dominated by the S_2 mode. At the same time, modes A_2, A_3 and S_3 generated at the edge of the excitation interval have smaller signals because of the frequency mismatch. These modes and the S_2 mode together form an HOMC that propagates forward.

To demonstrate the different frequency effect on the inspection results, a higher frequency of 3.96 MHz was selected from Figure 2 to excite mainly the S_3 mode and demonstrate the frequency effect on the inspection results. The excitation region is shown in gray. To generate the S_3 mode, a double-layer rectangular coil with a 0.75-mm coil spacing was designed and fabricated to perform the tests.

3.2 Experimental System

Figure 3 shows the experimental system for the HOMC Lamb waves inspection of pinhole defects using EMATs. Nine-cycle sine waves were generated by a waveform

generator (Agilent 33500B) and then amplified to 500 V using a power amplifier (Model 75A250A, Arworld, USA) to drive the transmitting transducer. The Lamb waves excited by the transducer propagated through the specimen and reached the receiving transducer to form a response signal. The response signal was amplified using a self-developed signal amplifier (North University of China, China) and recorded using a signal collector (HandyScope HS5, TiePie Engineering, USA). All the signals analyzed in this study were acquired at a sampling rate of 200 MHz. The transmitting and receiving EMATs were the same and consisted of a square permanent magnet and meander-line coils. The permanent magnet material was NdFeB dimensions of 30 mm × 30 mm × 30 mm (length × width × height). The meander-line coils were printed on a PCB board with spacing of 1.0 and 0.75 mm for the 2.87 and 3.96 MHz, respectively. The excitation voltage was 500 V for both the conventional and STR inspections.

3.3 Specimen Preparation

Artificial micro-holes were machined to simulate actual corrosion defects. The inspected specimen used in this study was an aluminum plate with the dimensions 1000 mm × 600 mm × 3 mm (length × width × thickness). The transmitting and receiving transducers were located at the straight line parallel to the length direction of the plate. The distances from the transmitting and receiving transducers to the left boundary of the aluminum plate were 250 and 400 mm, respectively. All pinhole defects were aligned in a vertical line 500 mm from the left boundary. Two specimens, named as Specimens #1 and #2, were inspected as shown in Figure 4. The pinhole defects were machined by a micro-milling process to guarantee the accuracy of the size and position. In Specimen #1, five pinholes were machined with decreasing diameters from 5 to 1 mm in steps of 1 mm. The 3-mm depth of the pinholes was used to test the sensitivity of the STR inspection of the Lamb waves mode to the defect size. Hole #3 was located at the extension line

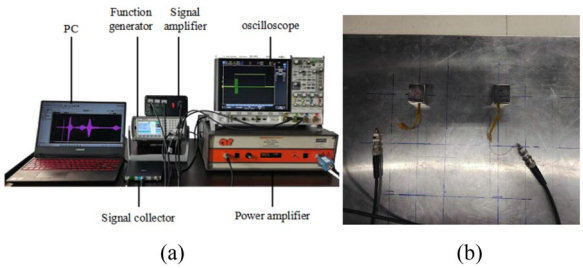

Figure 3 Experimental setup: **a** Overview of the system and **b** configuration of the EMATs and specimen

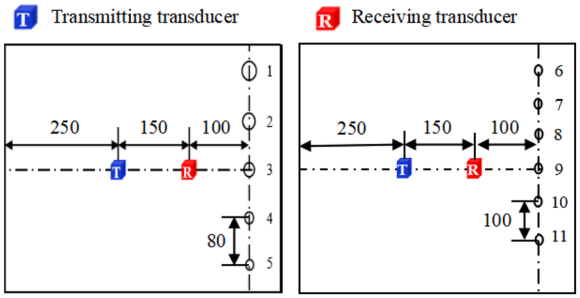

Figure 4 Configuration of the transducers and pinhole positions

between the transmitting and receiving transducers, and the distance between holes was 100 mm. Specimen #2 had six pinholes with 0.5-mm diameters (Holes #6—#11) with the decreasing depths from 3 to 0.5 mm, which is used to test the sensitivity of the STR inspection of Lamb waves mode on defect depth. For Specimen #2, Hole #9 was located at the extension line between the transmitting and receiving transducers. The detailed positions and sizes of the pinholes are presented in Table 1 and Figure 4.

3.4 Experimental Procedure

To demonstrate the effectiveness of the STR higher order Lamb waves mode in the pinhole inspection, both the conventional and proposed methods were used to detect the defects in Specimens #1 and #2. The testing process is described as follows:

(1) Conventional inspection. A nine-cycle sine signal with a center frequency of 2.87 or 3.96 MHz is applied in the transmitting transducer to excite acoustic waves in the specimens. After the acoustic propagates to the receiving transducer, the inspection signal is received by the receiving transducers and recorded by the computer. Conventional inspection signals are processed using Gaussian filtering to remove noise for the defect identification and STR inspection.

Table 1 Pinhole size of two specimen

No.	Specimen #1	No.	Specimen #2
1	Φ5 mm × 3 mm	6	Φ0.5 mm × 3 mm
2	Φ4 mm × 3 mm	7	Φ0.5 mm × 2.5 mm
3	Φ3 mm × 3 mm	8	Φ0.5 mm × 2 mm
4	Φ2 mm × 3 mm	9	Φ0.5 mm × 1.5 mm
5	Φ1 mm × 3 mm	10	Φ0.5 mm × 1 mm
		11	Φ0.5 mm × 0.5 mm

(2) STR inspection. The signals received by conventional inspection are divided into several segments. The segmented signal is a TR used to generate a new excitation signal. The new excitation signals are then emitted to the receiving transducer, and the echo signal received by the transmitting transducer is saved in the computer for the defect inspection. The inspection signals are processed by Gaussian filtering to remove noise and avoid any influence on defect identification.
(3) Defects identification. The position of the defect echo is located, and the amplitude is extracted to compare the sensitivity and feasibility of the inspection methods.

A comparison of conventional and STR inspections for different defect sizes are discussed, and the effects of the segment window location and width on the STR inspection robustness are presented. Finally, the results from different excitation frequencies and powers are compared.

4 Results and Discussions

4.1 Comparison of Conventional and STR Inspections

Conventional inspection and STR inspection were carried out for Specimen #2 pinhole defects with a depth of 0.5 mm and a diameter of 0.5 mm. The smallest hole size chosen in this test was used to confirm the sensitivity of the STR inspection for pinhole detection. The filtered signals obtained using Gaussian filtering are shown in Figure 5. As shown in Figure 5(a), when using the conventional inspection method, the direct wave and left boundary echo were directly identified based on the structure of Specimen #2. According to the configuration of pinhole and transducer location, the pinhole echo signal was estimated to be in the range of 90−150 μs, as shown in the expanded area in the middle of Figure 5(a). The pinhole echo signal amplitude was small, obscured by noise, and difficult to distinguish. The amplitude of the pinhole echo was 0.03722 V, and the inspection effectiveness was poor.

The conventional inspection signals from 75 to 150 μs, which include the defect signal, were divided into three segments indicated by red, green, and blue rectangles (Segments 1, 2, and 3, respectively) for the STR inspection. The signal in Segment 1 contained only white noise. The signal in Segment 2 contained both white noise and defect echo information, and the signal in Segment 3 contained white noise and an unknown noise (possibly from the measurement instrument). Each segment of a signal is a TR to obtain a new excitation signal. The results are shown in Figure 5(b), (c), and (d), where the picture on the left is the signal after TR, the regional amplified signal in the middle, and the time reversal factor (TRF) for each segment on the right. After zooming in on the TR signal by Segment 1 of Figure 5(b), a defect echo signal appeared with an amplitude of 0.06823 V, which was larger than that of the conventional inspection. This defect echo was generated by the TR signal transmitted through the pinhole, and the increased amplitude was the result of the enhanced noise signal overlapping the defect echo. The identified defect echo signal from the STR inspection by Segment 2 shown in Figure 5(c) had an amplitude of 0.1139 V. Compared to the conventional inspection, the defect echo amplitude increased by 206% owing to the focusing performance of the TR inspection method. For the unknown noise in Segment 3, the noise amplitude was also enhanced as shown in Figure 5(c); however, the wave package was dispersed and easily recognized as noise. From the above comparisons, the STR inspection enhanced the defect echoes and facilitated defect echo detection, even if the noise was also enhanced to some degree.

Figure 5(e) shows the STR inspection results using the conventional inspection signal from 75 to 175 μs, which is the entire truncation window without segmentation. The defect echo amplitude was 0.136 V and was 20% larger than the 0.1139 V amplitude of the STR in Figure 5(c). Moreover, the SNR of the entire truncation window inspection result without segmentation was 19.31 dB and was no better than the 20.30 dB of the STR. This result indicates that the segmentation process in STR inspection does not affect the inspection sensitivity and accuracy. Furthermore, each STR inspection can save 2/3 opening time for high-power amplifiers compared to conventional TR inspection. If the segmentation is N, the opening time of high-power amplifier is only 1/N. Thus, the STR can achieve high duty cycle, which is very important for minimizing instrument volume and power consumption. More importantly, the STR method does not need to know the approximate location of defect echo in the signal in advance. This advantage will be explained in detail in Section 4.2.

After completing the inspection of pinhole defects in Specimens #1 and #2 by both the conventional and STR methods, the amplitudes of the echo peaks were extracted and compared as shown in Figure 6. When the pinhole depth changed from 0.5 to 3 mm at the same 0.5 mm diameter, the pinhole amplitudes from both conventional and STR inspections increased. This phenomenon indicates that the smaller the defect, the harder it is to detected. However, the pinhole amplitudes of the conventional inspection were in the range of 0.02−0.08 V and were easily obscured by 0.01 V white noise. The superiority of STR inspection is obvious for micro-sized defects, in which the defect echo amplitude was

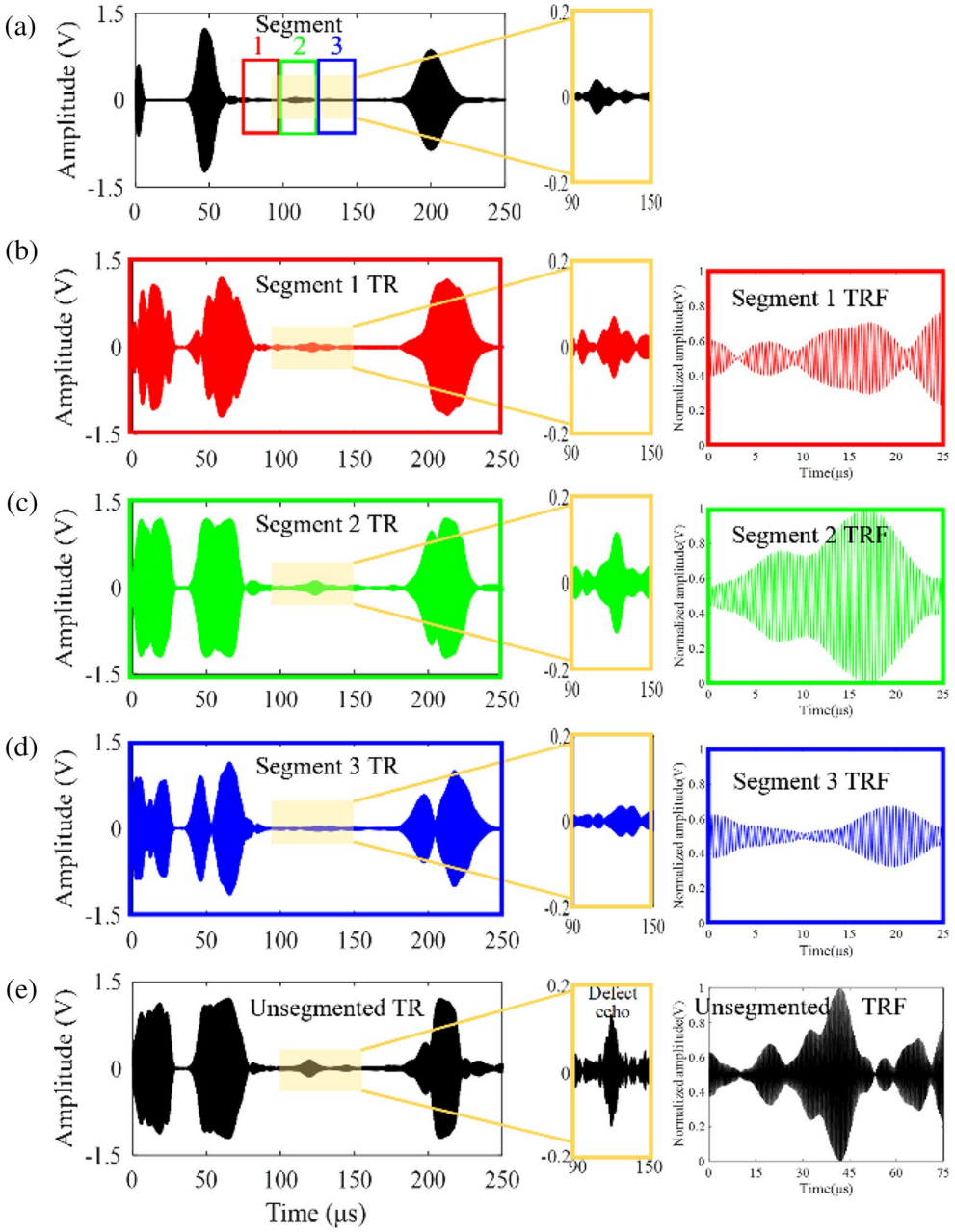

Figure 5 2.87 MHz detection results: **a** Conventional inspection, STR inspection with **b** Segment 1, **c** Segment 2, **d** Segment 3, and **e** unsegmented time reversal method

increased by approximately four times and the SNR range increased from 2−8 dB to 10−30 dB. The STR inspection results for pinhole defects with a 3 mm depth and different diameters were similar to those for pinhole defects with a 3 mm diameter and different depths. STR inspection improves defect detection, particularly for micro-sized defects with very low defect echo amplitudes easily obscured by noise.

4.2 Influence of Segment Window Location

When setting an STR window, the conventional defect echo may be included in one segment or separated by two adjacent segments. When a conventional defect echo is completely within a window, as shown in Figure 5, the TR defect echo is only effectively enhanced in the segment window including the defect echo. The segment window without the conventional defect echo

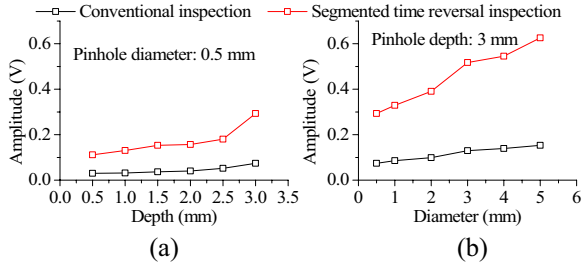

Figure 6 Comparison of conventional and STR methods under different defects **a** in depth and **b** in diameter

enhanced only the noise. When a defect echo is separated by two adjacent segments, three assumptions are made:

Assumption A: Most of the defect echo signal is in the former segment;

Assumption B: The defect echo signal is separated by two segments equally;

Assumption C: The majority of the defect echo signal is in the later segment.

Figure 7 shows the STR inspection results for Assumption A. A strong defect echo was found by the STR inspection by Segment 1 that contained most of the conventional defect echo signal. The amplitude of the defect was 0.1203 V and was similar to the results of the conventional defect echo shown in Figure 5(c). The STR result processed by Segment 2 also had a visible defect echo owing to part of the conventional defect echo, as shown in Figure 7(b). The amplitude was 0.05221 V and was 40% larger than that of the conventional defect echo. Figure 7(b) shows the enhancement of noise because Segment 3 contains the noise of the conventional inspection signal. An envelope comparison is shown in Figure 7(c).

Figure 8 shows the STR inspection results under Assumption B, in which the conventional defect echo was equally separated by two adjacent windows. As shown in Figure 8(a), the direct defect echo was separated into Segments 1 and 2. The STR results by Segments 1 and 2 presented in Figure 8(b) show that the echo signals were enhanced in both conditions. The amplitudes of the defect echoes were 0.08814 and 0.07702 V, increases of 136% and 106%, respectively, compared with the conventional inspection. The STR signal by Segment 3 was slightly larger than that of the conventional inspection results because the enhanced noise signal overlapped with the defect echo in the reversal pinhole echo information.

The STR inspection results when the majority of the conventional defect echo signal was in Segment 2, which is Assumption C, are shown in Figure 9. The

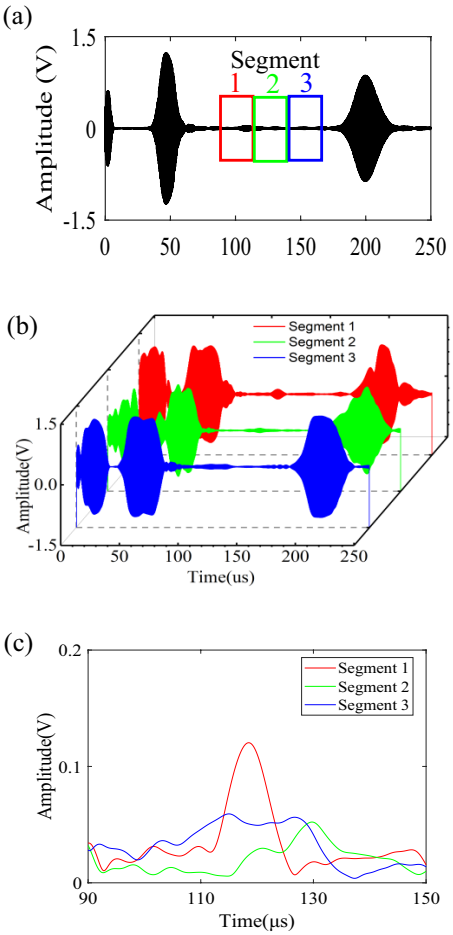

Figure 7 Detection results under Assumption A: **a** Signal segmentation, **b** STR inspection results by Segments 1, 2, and 3, and **c** envelope comparison of different segments

defect echo of the STR by Segment 1 was slightly enhanced as shown in Figure 9(b). The STR signal by Segment 2 detected the pinhole, and the echo signal amplitude was enhanced to 0.07705 V. The defect echo signal amplitude increased by two times compared with that of conventional inspection. Segment 3 showed no change in the enhancement of noise.

Based on the above results, regardless of whether the conventional defect echo was in one segment window or separated by two adjacent windows, the STR inspection signal was enhanced compared to that of conventional inspection. When one segment contained complete defects, STR Lamb waves focused on the defect and enhanced the echo energy of the defect. When a defect was located on two adjacent segments, both STR signals detected the defect echo and enhanced the amplitude. The more defect echo contained in a segment, the higher the defect echo amplitude detected by the STR

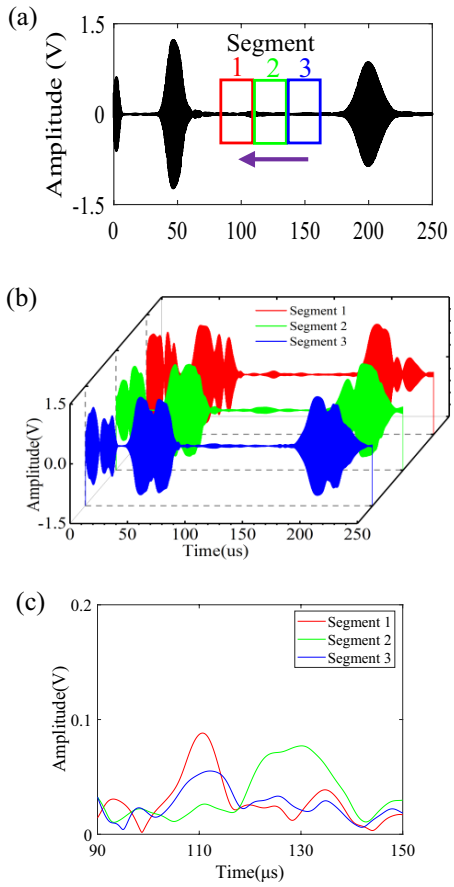

Figure 8 Detection results under Assumption B: **a** Signal segmentation, **b** STR inspection results by Segments 1, 2, and 3, **c** envelope comparison of different segments

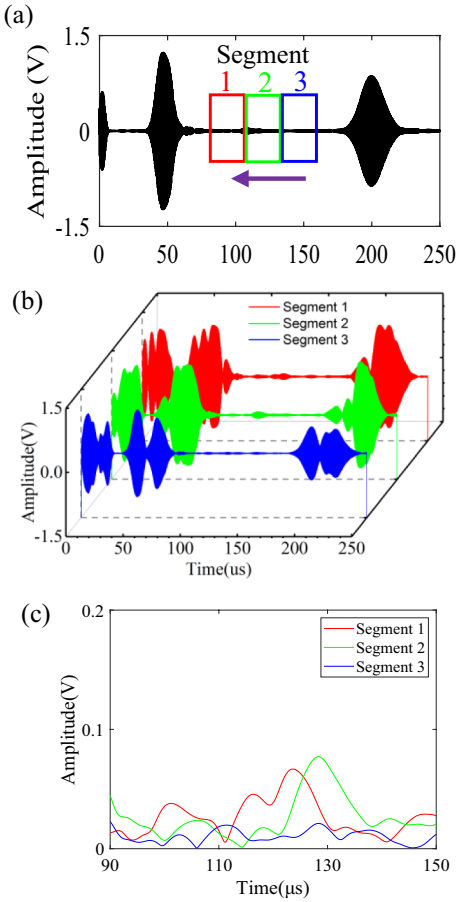

Figure 9 Detection results under Assumption C: **a** Signal segmentation, **b** STR inspection results by Segments 1, 2, and 3, and **c** envelope comparison of different segments

inspection; even when a conventional defect echo was divided into two adjacent segments, the inspected defect still had a larger amplitude.

4.3 Influence of Segmented Window Width

When setting the window width, a larger window width consumes more opening time of the high-power amplifier. An unnecessary window width reduces the SNR because the noise signal is enhanced. In contrast, a smaller window width may lose some useful information and reduce the sensitivity of the signal. The selection of the segmented window width increases the difficulty of the detection tasks and the requirements of inspectors.

Figure 10 illustrates the effect of the segmented window width on inspection results. The SNR was chosen as the parameter to assess the segmented window width effect. The segmented window widths were increased from 5 to 35 μs with an interval step of 5 μs. The STR inspection signal of a pinhole Φ0.5 mm × 0.5 mm was used to calculate the SNR. With an increase in the

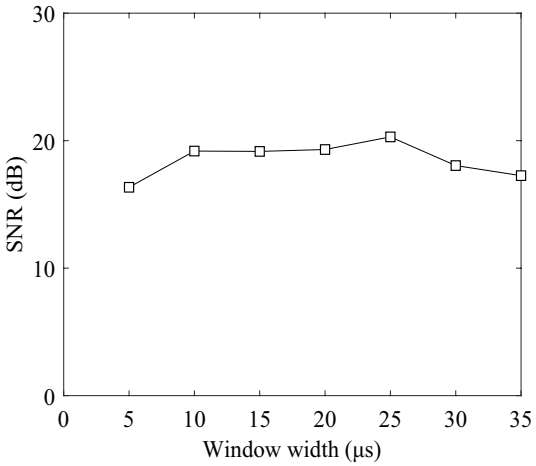

Figure 10 SNR when setting different window widths

segmented window width, the SNR first increased from 5 to 25 μs and then decreased when the width was larger than 25 μs. The maximum SNR was 20.30 dB with a 25 μs segmented window width. The SNR discrepancy of 10–25 μs was very small (less than 10%) and acceptable. The SNR of window widths less than 10 μs or larger than 25 μs decreased by more than 20% compared to those in 10–25 μs range. Time duration of conventional excitation signal used in this experiment was 3.13 μs. Considering the superposition of the energy of multiple modes and the frequency dispersion of the modes, when using the TR method, a short TR window width includes a small energy and the function of the TR method cannot be effectively applied, while a long TR window width leads to significant noise and is not conducive to detection. Combined with the experimental results, the window width of the TR method was 5–10 times that of the conventional excitation signal, and a signal duration of eight times was selected for detection in this study.

4.4 Comparison of Different Excitation Frequencies and Power Detection

The HOMC method shows high sensitivity to micro-sized defects. To optimize the detection processes, the excitation frequency can be increased to determine the consistency of the HOMC method. Figure 11(b) shows the detection results obtained by setting a central frequency of 3.96 MHz. The amplitudes of the conventional and STR inspections were 0.03322 and 0.198 V, respectively. Only the enhanced segment result was considered. The signal of the STR inspection increased by six times compared to that of the conventional inspection, further proving the versatility of the STR inspection at higher frequencies. Compared with the result at 2.87 MHz in Figure 5(a), the pinhole amplitudes increased by approximately 20% and 54% for conventional and STR inspection, respectively. These results indicate that a higher excitation frequency combined with the TR method improved the inspection sensitivity and enhanced the ability to detect micro-sized defects. However, a higher excitation frequency increases the bandwidth demand of inspection system and needs to be further investigated in future work.

Excitation power is another variable in the inspection. Theoretically, a higher excitation power can yield a better defect echo signal because more energy is transferred to the inspection system. However, high excitation power requires a powerful amplifier which may not be available in practice. Moreover, a high excitation power is not feasible for the containers with inflammable and explosive medium. An amplifier with a lower output power can reduce the difficulty of instrument development, save energy on specific occasions, and is more practical in industrial applications for safety reason.

Figure 12(a) and (b) show the conventional and STR detection result of Φ0.5 mm × 0.5 mm

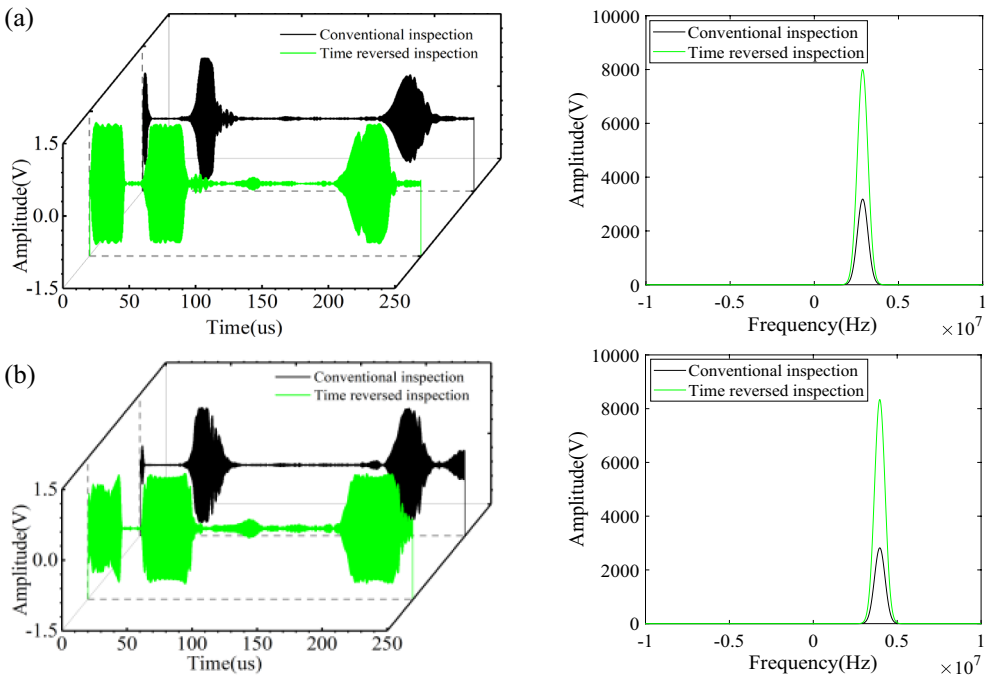

Figure 11 Inspection signals of Φ0.5 mm × 0.5 mm defects: **a** Comparison at 2.87 MHz and frequency spectrum, **b** comparison at 3.96 MHz and frequency spectrum

(diameter × depth) pinhole defects at 500 V and 2.87 MHz without and with artificial noise, the results show that the STR method had an obvious focusing effect and strong suppression effect on noise under high voltage scenario. Figure 12(c) shows the detection result of Φ0.5 mm × 0.5 mm (diameter × depth) pinhole defects at 250 V and 2.87 MHz. Pinhole defects echoes are obscured by noise and cannot be detected by conventional detection when the excitation voltage is 250 V. After STR inspection, the pinhole defect echoes were enhanced and detected with an amplitude of 0.0551 V and SNR was 22.16 dB. In addition, compared to the detection result at 500 V and 2.87 MHz as shown in Figure 5(a), SNR at 250 V was increased by 1.86 dB.

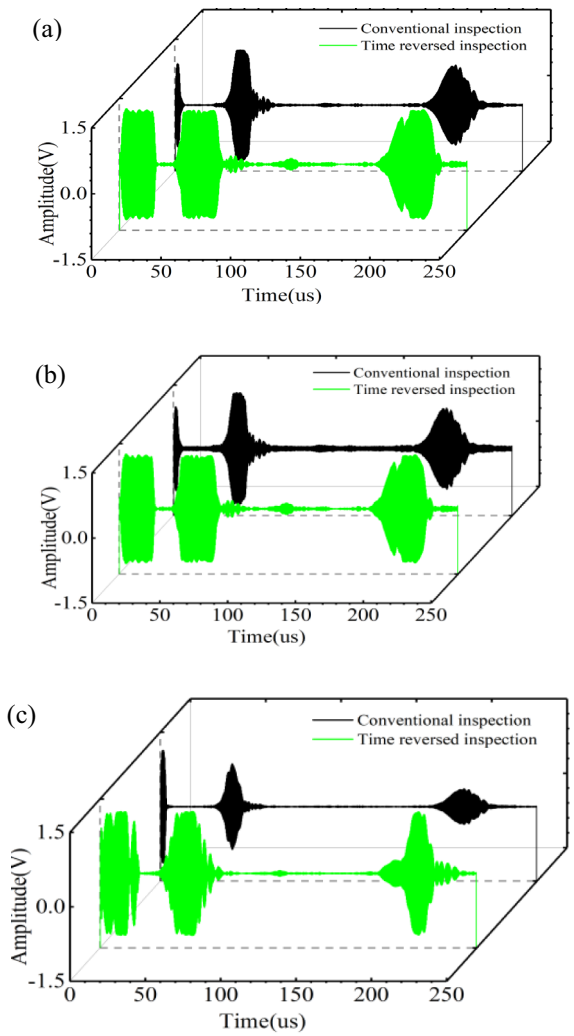

Figure 12 Pinhole defect detection: **a** Comparison at 500 V, **b** comparison of segmented method at 500 V with noise, and **c** STR detection at 250 V

Figure 12(c) was a convincing and meaningful experimental result. Because low power excitation lead to low SNR. However, it's not an additive noise but systematic electrical noise. The reduction of voltage affects the energy conversion of the whole system. Especially for EMATs detection system, the instrument noise generated by low energy conversion efficiency is unavoidable and difficult to process. The result indicates that the STR can deal with different kind of noise even for micro-size defects and the performance is better than normal high voltage. So, the STR method can improve the sensitivity and robustness of low-power detection and reduce the requirements for hardware performance of testing instruments to benefit practical applications. The STR-HOMC inspection is more suitable for micro-sized corrosion and has good stability and adaptability, particularly under low power safety scenario.

5 Conclusions

An STR detection method based on the HOMC method was proposed and the effectiveness was verified in experimentally. The conclusions drawn are as follows:

(1) The HOMC is an effective method to detect inaccessible areas with high resolution. And EMATs is beneficial to exciting higher order modes of different frequencies. Also, focusing method can improve the SNR for EMATs. The combination of these methods with specific design for excitation frequency and TR window improves the detection sensitivity and enhances the ability to detect minor defects, which proves the consistency and effectivity of the HOMC method.

(2) Innovative STR detection can achieve spatio-temporal focusing and obtain two obvious advantages. First, STR detection enhances the ability to detect smaller defects with four times performance improvement. Second, STR method overcomes the shortcomings of the normal TR methods that are difficult to determine the starting point of a narrow TR window. No matter the defect signal is divided by STR window at any position, the window containing defect signal can always achieve the focusing effect at the defect. So the selection of window width position has no influence on the defect detection.

(3) The segmented method is more suitable for low power scenario from two perspective views. From one perspective, it can improve the sensitivity and robustness of detection even for systematic noise. Another one is that, the opening time of amplifier can be significantly reduced. This benefit reduces hardware and power requirements of testing instru-

ments, which is more suitable for micro-sized corrosion detection in safety critical industrial applications.

Acknowledgements
Not applicable.

Authors' Contributions
JZ provided guidance for the whole research, designed the experiment, and wrote the first draft. YH and SY performed the experiments and analyzed the data. YZ establish the experimental platform. LX and LY have polished up the manuscript. All authors read and approved the final manuscript.

Authors' Information
Jinjie Zhou, born in 1981, received his PhD degree from *Beijing University of Technology* in July 2012. He is now an associate professor at *School of Mechanical Engineering*, *North University of China*. At present, he is mainly engaged in the research of material properties analysis and detection methods in an extreme environment, the key technology research of instruments, and the development of automatic measurement and control systems.
Yang Hu, born in 1998, is currently a master candidate of *North University of China*. In 2021, he received his bachelor's degree in mechanical design, manufacturing and automation from *North University of China*.
Xiang Li, born in 1982, received the PhD degree from *University of Electronic Science and Technology of China (UESTC)* in 2012. He is currently an associate professor of *Faculty of Aeronautics and Astronautics, UESTC*. His research interests include nondestructive testing and evaluation and related signal processing method, and machine learning method.
Yang Zheng, born in 1984, received his B. Sc. degree in mechanical engineering and automation from *Beihang University* in 2007, and Ph.D. degree in mechanical engineering from *Beijing University of Technology* in 2012. Now, he currently works as a research fellow at *China Special Equipment Inspection and Research Institute*. His research interests include nondestructive testing and evaluation techniques, instrument development, and standards development.
Sanhu Yang, born in 1997, received his master's degree from *North University of China* in 2022, majoring in electromagnetic ultrasonic guided waves detection.
Yao Liu, born in 1990, received his PhD degree from *Donghua University* in 2018. He is now an associate professor at *School of Mechanical Engineering*, *North University of China*. His research areas are ultra-precision machining and ultrasonic inspection technology.

Funding
Supported by National Natural Science Foundation of China (Grant No. 62071433) and National Key R&D Program of China (Grant No. 2022YFC3005002).

Competing Interests
The authors declare no competing financial interests.

Received: 11 July 2022 Revised: 12 January 2023 Accepted: 31 January 2023
Published online: 23 February 2023

References

[1] M S Rabbi, K Teramoto, H Ishibashi, et al. Imaging of sub-surface defect in CFRP laminate using A0-mode Lamb wave: Analytical, numerical and experimental studies. *Ultrasonics*, 2022, 127: 106849.
[2] H L Chen, K L Xu, Z H Liu, et al. Ellipse of uncertainty based algorithm for quantitative evaluation of defect localization using Lamb waves. *Ultrasonics*, 2022, 125: 106802.
[3] Z H Liu, Y N Hu, M W Xie, et al. Development of omnidirectional A(0) mode EMAT employing a concentric permanent magnet pairs with opposite polarity for plate inspection. *NDT & E International*, 2018, 94: 13-21.
[4] Z H Liu, L M Deng, Y C Zhang, et al. Development of an omni-directional magnetic-concentrator-type electromagnetic acoustic transducer. *NDT & E Internationa*, 2020, 109: 102193.
[5] Z H Liu, L M Deng, Y C Zhang, et al. Development of a mode-tuning magnetic-concentrator-type electromagnetic acoustic transducer. *Ultrasonics*, 2020, 103: 106094.
[6] Z Abbasi, F Honarvar. Evaluation of the sensitivity of higher order modes cluster (HOMC) guided waves to plate defects. *Applied Acoustics*, 2022, 187: 108512.
[7] L M Campeiro, D E Budoya, F G Baptista. Lamb wave inspection using piezoelectric diaphragms: An initial feasibility study. *Sensors and Actuators: A. Physical*, 2021, 331: 112859.
[8] Y S Sun, Y F Xu, W Li, et al. A Lamb waves based ultrasonic system for the simultaneous data communication, defect inspection, and power transmission. *IEEE Transactions on Ultrasonics, Ferroelectrics, and Frequency Control*, 2021, 68(10): 3192-3203.
[9] K Song, J H Kwak, J J Park, et al. Acoustic metasurfaces for efficient matching of non-contact ultrasonic transducers. *Smart Materials and Structures*, 2021, 30(8): 085011.
[10] D Ratnam, K Balasubramaniam, B W Maxfield. Generation and detection of higher-order mode clusters of guided waves (HOMC-GW) using meander-coil EMATs. *IEEE Transactions on Ultrasonics, Ferroelectrics, and Frequency Control*, 2012, 59(4): 727-737.
[11] Nurmalia, N Nakamura, H Ogi, et al. EMAT pipe inspection technique using higher mode torsional guided wave T(0, 2). *NDT & E International*, 2017, 87: 78–84.
[12] Z H Liu, X Zhao, J Q Li, et al. Obliquely incident EMAT for high-order Lamb wave mode generation based on inclined static magnetic field. *NDT & E International*, 2019, 104: 124-134.
[13] S H Reddy, A Vasudevan, P Rajagopal, et al. Scattering of higher order mode clusters (HOMC) from surface breaking notches in plates with application to higher temperature gradients. *NDT & E International*, 2021, 120: 102441.
[14] R Gangadharan, C R L Murthy, S Gopalakrishnan, et al. Time reversal technique for health monitoring of metallic structure using Lamb waves. *Ultrasonics*, 2009, 49(8): 696-705.
[15] Y Y Zhang, D S Li, Z Zhou, et al. Time reversal method for guided waves with multimode and multipath on corrosion defect detection in wire. *Applied Sciences*, 2017, 7(4): 424.
[16] J Harley, N O'Donoughue, Y Jin, et al. Time reversal focusing for pipeline structural health monitoring. *Proceedings of Meetings on Acoustics*, 2010, 8(1): 030001.
[17] L Q Guan, W G Zhu, Y F Li. Research on hybrid techniques of time-reversal ellipse location and tomographic imaging of Lamb wave. *Journal of Nanjing University (Natural Science)*, 2019, 55(2): 191-201. (in Chinese)
[18] Y Xu, M Z Luo, Q Liu, et al. PZT transducer array enabled pipeline defect locating based on time-reversal method and matching pursuit denoising. *Smart Materials and Structures*, 2019, 28(7): 075019.
[19] H F Zhang, S H Cao, S W Ma, et al. Multi-sensor network for industrial metal plate structure monitoring via time reversal ultrasonic guided wave. *Measurement*, 2020, 152(C): 107345.
[20] C G Fan, S Q Yu, B Gao, et al. Ultrasonic time-reversal-based super resolution imaging for defect localization and characterization. *NDT & E International*, 2022, 131: 102698.
[21] J C Vallée, M A Ploix, F Baqué, et al. Edge and notch detection in a plate using time reversal process of leaky Lamb waves. *Applied Sciences*, 2021, 12(1): 228.
[22] N Saber, L Moez, G M Murat, et al. Time-reversal techniques for defect detection in pipe system using high frequency acoustic waves. *The Journal of the Acoustical Society of America*, 2019, 146(4): 2867-2867.
[23] I Petromichelakis, C Tsogka, C G Panagiotopoulos. Signal-to-noise ratio analysis for time-reversal based imaging techniques in bounded domains. *Wave Motion*, 2018, 79: 23-43.
[24] H Sohn, H W Park, K H Law, et al. Damage detection in composite plates by using an enhanced time reversal method. *Journal of Aerospace Engineering*, 2007, 20(3): 141–151.
[25] B L Xu, V Giurgiutiu. Single mode tuning effects on lamb wave time reversal with piezoelectric wafer active sensors for structural health monitoring. *J. Nondestr Eval.*, 2007, 26(2): 123-134.

[26] B Poddar, A Kumar, M Mitra, et al. Time reversibility of a Lamb wave for damage detection in a metallic plate. *Smart Mater. Struct.*, 2011, 20(20): 025001.
[27] J K Agrahari, S Kapuria. Effects of adhesive, host plate, transducer and excitation parameters on time reversibility of ultrasonic Lamb waves. *Ultrasonics*, 2016, 70: 147-157.
[28] L P Huang, L Zeng, J Lin, et al. An improved time reversal method for diagnostics of composite plates using Lamb waves. *Composite Structures*, 2018, 190: 10-19.
[29] C G Fan, L Yang, Y Zhao. Ultrasonic multi-frequency time-reversal-based imaging of extended targets. *NDT & E International*, 2020, 113: 102276.
[30] R H Jiang, Z G Song, C Zheng, et al. Time reversal ESPRIT imaging with frequency-domain sampling of single target. *IOP Conference Series: Materials Science and Engineering*, 2018, 466(1): 012044.
[31] F Deng, B Wu, C F He. Time reversal guided wave defect identification method. *Journal of Mechanical Engineering*, 2010, 46(8): 18-24. (in Chinese)
[32] F Deng. A time reversal guided wave inspection method based on one signal generator tunnel. *Journal of Mechanical Engineering*, 2011, 47(6): 17–21. (in Chinese)
[33] M Kannusamy, S Kapuria, S Sasmal. An efficient Lamb wave-based virtual refined time-reversal method for damage localization in plates using broadband measurements. *Ultrasonics*, 2022, 124: 106767.